Electronic Supplementary Material (ESI) for Journal of Materials Chemistry

Supporting Information

Synergism of Interparticle Electrostatic Repulsion Modulation and Heat-induced Fusion: A Generalized One-Step Approach to Porous Network-like Noble Metal and Its Alloy Nanostructures

Jianhua Cui, Hua Zhang, Yifu Yu, Yang Liu, Yiling Tian, Bin Zhang*

Department of Chemistry, Tianjin University, Tianjin 300072, P. R. China

E-Mail: bzhang@tju.edu.cn

a) Schemat illustrating the self-assembly morphology of charged nanoparticles (NPs) via modulating the balance of long-range electrostatic repulsion potential (V_{elec}) and van der Waals attraction (V_{vdw})

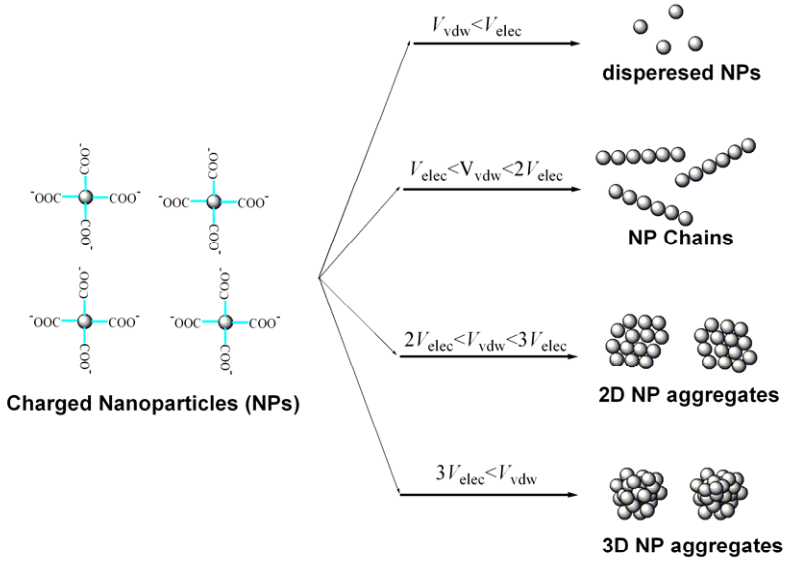

b) Fusion of particles

c) Anisotropic dipolar interaction induced fusion of particles at air-liquid interface

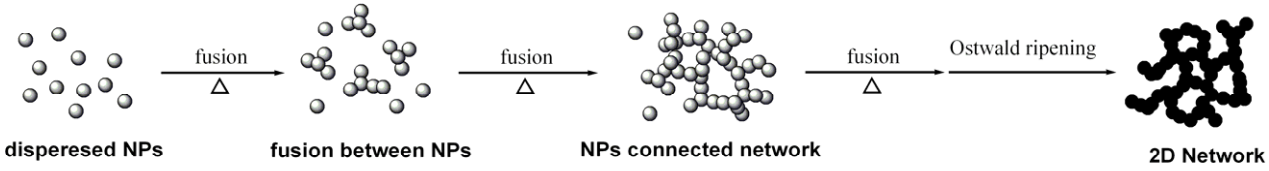

d) Two methods to lower V_{elec}

1. adding polar solvent with lower a smaller dielectric constant, such as ethylene glycol (EG), ethanol, acetonitrile, acetone, and *N,N*-dime thylformamide (DMF), to the charged-NPs-containing aqeous solution.

2. adding inorganic salt (e.g. NaCl, KCl) to the charged-NPs-containing aqeous solution.

Scheme S1. (a) Schematic depiction of self-assembly mode of charged nanoparticles endorsed by a balance between electrostatic repulsion (V_{elec}) and van der Waals attraction (V_{vdw}) between the particles in the presence of dipolar attraction force. The scheme is drawn on the basis of the theoretic calculation and discussion of Au NPs (Zhang, H.; Wang, D. *Angew. Chem. Int. Ed.* **2008**, *47*, 3984–3987). (b) Scheme illustrating the mode of the fusion of particles into larger particles. (c) Scheme showing the formation of 2D porous network dominated by the dipolar interaction and interparticle fusion of charged NPs at air-liquid interface. (d) Two ways to lower V_{elec} of charged seeds proposed according to Derjaguin-Landau-Verwey-Overbeek (DLVO) theory (Israelachvili, A J. Intermolecular & Surface Forces, Academic Press, London, **1997**.) and calculated equation of V_{elec} that Wang and his coworker suggested (Zhang, H.; Wang, D. *Angew. Chem. Int. Ed.* **2008**, *47*, 3984–3987). In this communication, we will extent the thermodynamic control technique of NPs assembly to the nucleation and growth process of metal and alloy nanostructures, and develop a general one-step method to fabricate 3DPNN of metals and alloys.

The colloidal stability of charged particles (NPs) or seeds in an aqueous medium is estimated by using the Derjaguin–Landau–Verwey–Overbeek (DLVO) theory [Israelachvili, A J. Intermolecular & Surface Forces, Academic Press, London, 1997.]. For monodispersed spherical NPs, V_{elec}, V_{vdW}, $V_{charge-dipole}$ and V_{dipole} can be calculated as shown in Equations (1)–(4). The total interaction potential (V_T) is expressed as the sum of the electrostatic repulsion potential (V_{elec}), the van der Waals attraction potential (V_{vdW}), the charge–dipole interaction potential ($V_{charge-dipole}$), and the dipolar interaction potential (V_{dipole}) [Eq. (5)] [Zhang, H.; Wang, D. *Angew. Chem. Int. Ed.* **2008**, *47*, 3984–3987]. The V_{dipole} of charged NPs is usually negligibly small. Thus, the stability of charged NPs (seeds in our case) is mainly determined by the balance of V_{vdW} and V_{elec}[Zhang, H.; Wang, D. *Angew. Chem. Int. Ed.* **2008**, *47*, 3984–3987]. Wang and his coworkers have found that charged Au NPs are well dispersed when V_{elec} is larger than V_{vdW}, and are able to be assembled into one-dimensional chains ($V_{elec}<V_{vdw}<2V_{elec}$), and three-dimensional (3D) aggregates ($3V_{elec}<V_{vdw}$) by modulating the V_{elec} [Zhang, H.; Wang, D. *Angew. Chem. Int. Ed.* **2008**, *47*, 3984–3987], as shown Scheme S1a. According to Equations (1) and (3), a decrease in the dielectric constant of the medium surrounding the charged NPs can cause a decrease V_{elec} while V_{dipole} increases. It is known that the dielectric constant of water is 80.4 at 20 ºC. Thus, it is reasonable to expect that the addition of polar solvents with lower dielectric constant (ethylene glycol with a dielectric constant of 37 at 20 ºC or ethanol with a dielectric constant of 24.3), the as-formed charged seeds can assembled into 1D chain. The heat-induced fusion between neighboring seeds and 1D chain can lead to the formation of 3DPNN. However, big aggregates appeared when $3V_{elec}<V_{vdw}$ through adding enough ethylene glycol.

$$V_{elec}(r) = 2\pi\varepsilon_s\varepsilon_0\varphi_0^2 \ln\{1+\exp[-a\kappa(R-2)]\} \quad (1)$$

$$V_{vdw}(r) = -\frac{A_H}{6}\left[\frac{2}{R^2-4}+\frac{2}{R^2}+\ln\frac{R^2-4}{R^2}\right.$$

$$V_{charge\text{-}dipole}(r) = -\frac{Q^2\mu^2}{24(\pi\varepsilon_s\varepsilon_0)^2 k_B T r^4} \quad (3)$$

$$V_{dipole}(r) = -\frac{Q^2\mu^2}{2\pi\varepsilon_s\varepsilon_0 R(R^2-4a^2)} \quad (4)$$

$$V_T = V_{elec} + V_{vdw} + V_{charge\text{-}dipole} + V_{dipole} \quad (5)$$

[r is the center-to-center separation of neighboring NPs of radius a ($R=r/a$), ε_s is the relative dielectric constant of the solvent (about 80 for water), ε_0 is the dielectric constant of vacuum, Ψ_0 is the surface potential of the particle, μ is the dipole moment, κ is the inverse Debye length, k_B is the Boltzmann constant, T is the absolute temperature, Q is the effective surface charge of the NPs, and A_H is the Hamaker constant of the particles]

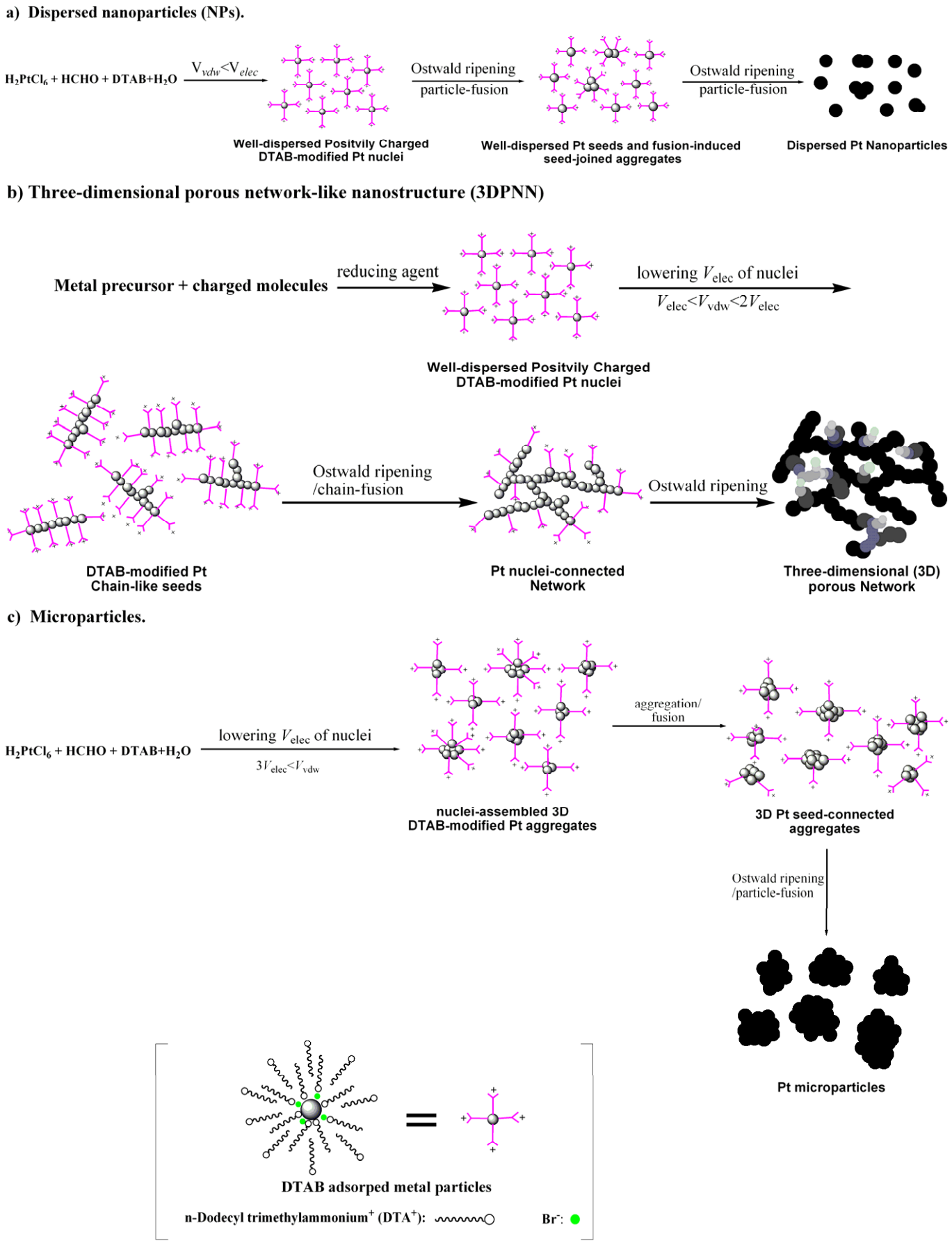

Scheme S2. (a-c) Schematic depiction of the formation process of dispersed NPs (a), 3DPNN (b) and microparticles (c). Pt 3DPNN were selected as the mode system to demonstrate the concept of the combination of interparticle fusion with the modulation of V_{elect} in controlling the morphology of metal

nanostructures. It is well known that metal precursors can be reduced by using HCHO to produce metal(0) under hydrothermal condition (*J. Am. Chem. Soc.* **2009**, *131*, 13916–13917.). DTAB, one of cation surfactants, was selected as adsorbed molecules to make the as-prepared metal nuclei and seeds be positively charged (*Chem. Mater.* 2003, *15,* 1957-1962. *Appl. Surf. Science* **2008**, *254*, 6289–6293). Ethylene glycol (EG) (or NaCl) was selected as polar solvent with lower dielectric constant (or salt), and added into the aqueous reaction solution to modulate the V_{elec} of metal nuclei and seeds. In the absence of EG (or NaCl), DTAB can adsorb on the surface of Pt nuclei and seeds, and make the as-formed Pt be positively charged. While the electrostatic repulsion force is stronger than V_{vdw} ($V_{elec}>V_{vdw}$), the interparticle repulsion interaction will dominate the nucleation and growth of Pt, and inhibit the aggregation and fusion between Pt particles, and thus lead to the formation of dispersed Pt NPs via Ostwald growth (Scheme S2a). On the other hand, the addition of salt (or polar solvent) can lower V_{elec} of Pt nuclei and seeds (Scheme S1). 1D chain-like assembly of nuclei and seeds will appear when V_{elect} is smaller than V_{vdw} while still larger than half of V_{vdw} ($V_{elec}<V_{vdw}<2\ V_{elec}$). The heat-induced fusion between NPs in 1D particle chains makes chains become rod-like structures. The Brownian motion may drive 1D particle chains coalescence. Then, the fusion among chains generates Pt 3DPNN, as shown in Scheme S2b and Figure 1). However, when the V_{vdw} is three times of V_{elec} with continuingly increasing the addition of NaCl (or EG) (Scheme S1), Pt seeds will agglomerate and fuse into bigger aggregates, finally the microparticles were produced, as displayed in Scheme S2c.

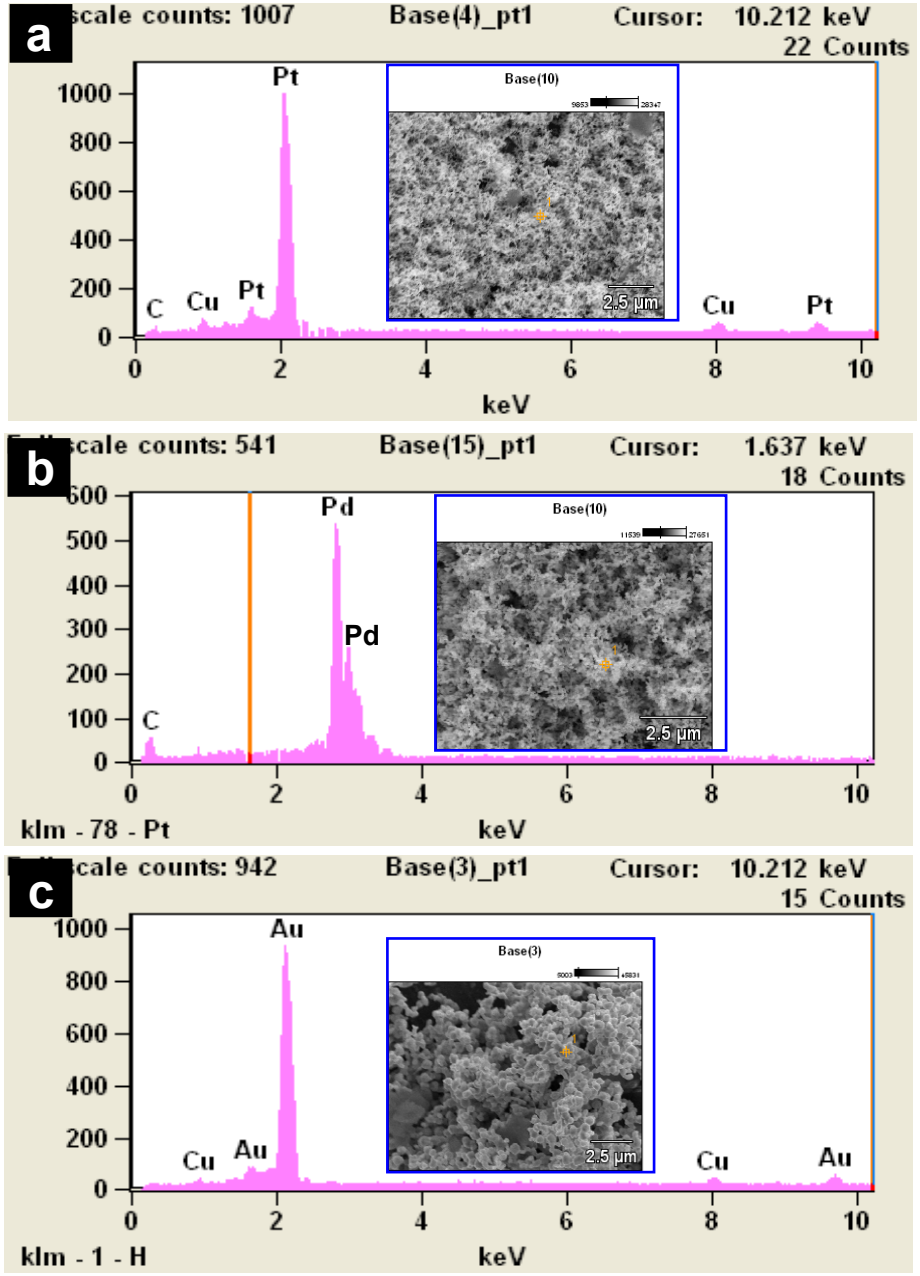

Figure S1. EDX spectra (a-c) and the associated SEM images (the insets) of the as-prepared Pt (a), Pd (b) and Au (c) 3DPNN, showing the samples are pure Pt, Pd and Au, respectively. In these EDX spectra, the detected Cu signals arise from the Cu foil on which the samples were deposited.

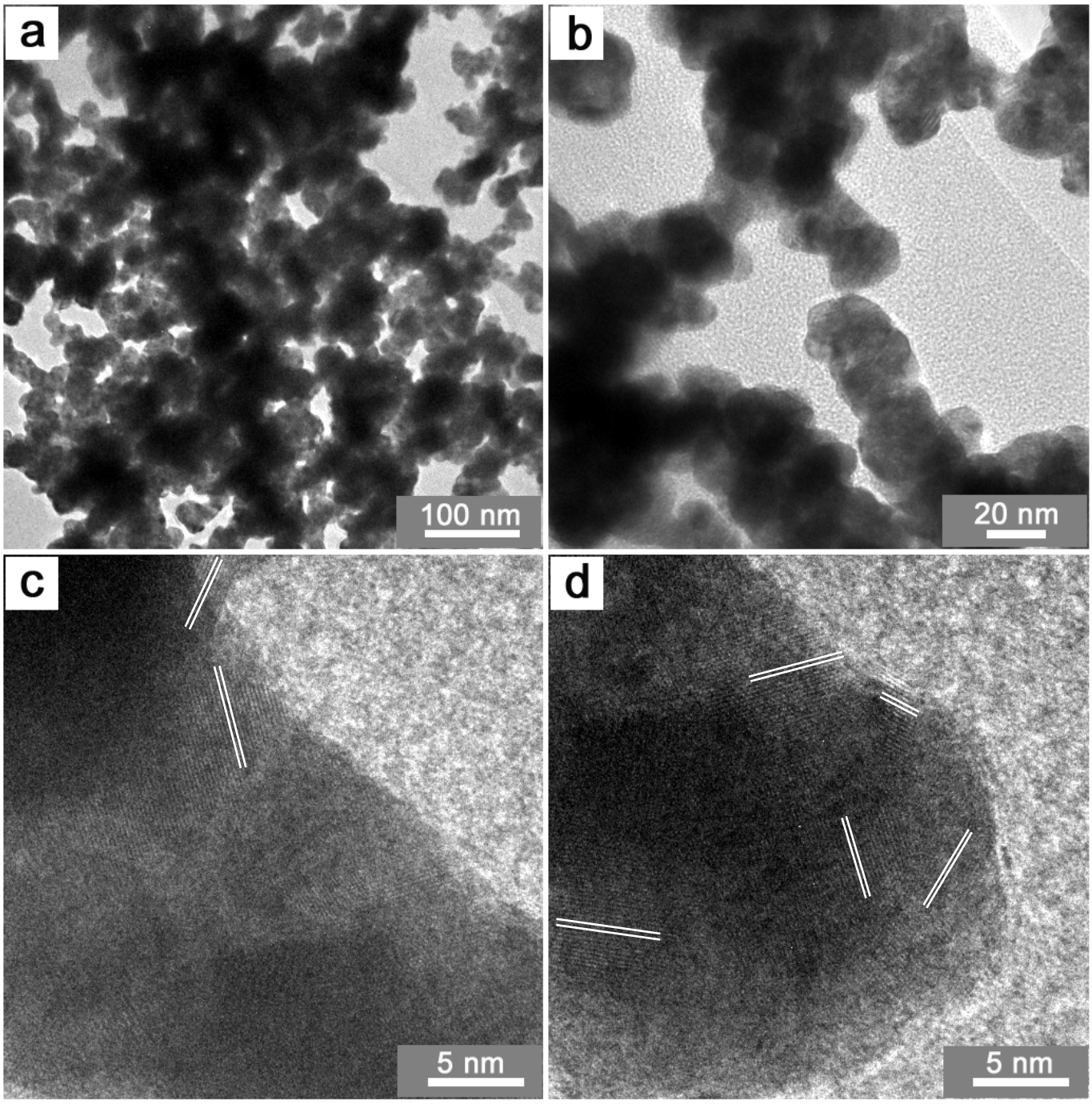

Figure S2-1. (a-b) TEM images of the as-prepared Pt 3DPNN, showing that the samples are 3D porous network-like structures composited of nanorod-like units. (c-d) HRTEM images of the as-prepared Pt 3DPNN. Clearly observed fringe spacing of 0.23 nm appearing in different directions (Figure S2-1d) suggests that the rod-like units may be generated through the interparticle fusion of Pt seeds and following ripening. In comparison with conventional single-crystal metal nanocrystals with smooth surface, the interparticle fusion may lead to the formation of the surface with more steps and corners, that is, active sites for catalytic reaction (G. Somorjai in *Advances in Catalysis*, *Vol. 26*, (Eds.: D. D. Eley), Academic Press Inc., New York, **1977**, pp. 2–68), as confirmed by the rough surface of rod-like units in 3DPNN in TEM images (Figure S2-1b). Thus, 3DPNN are expected to exhibit higher catalytic activity than single-crystalline nanocrystals and rods.

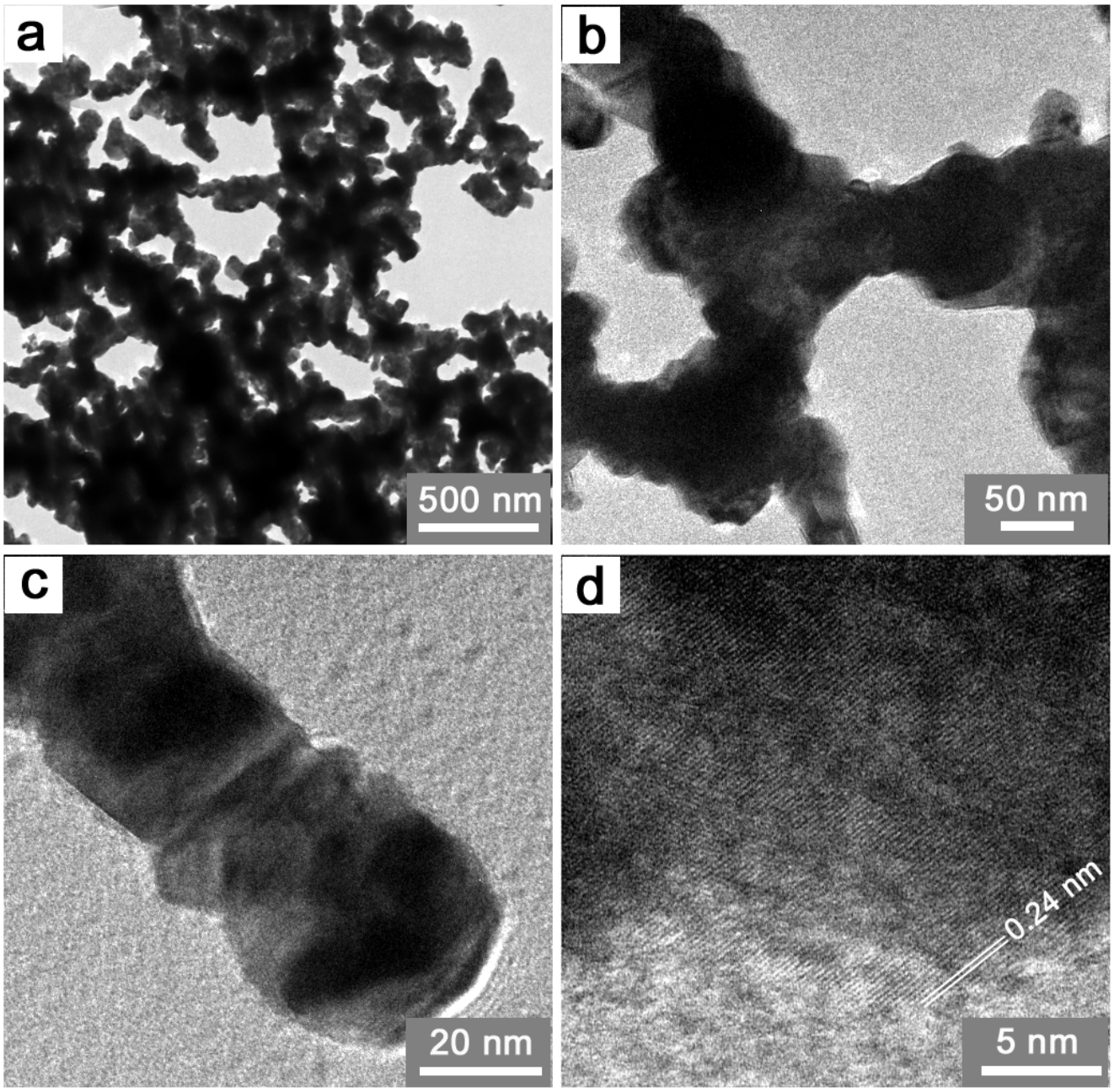

Figure S2-2. TEM images (a-c) and HRTEM (d) image of the as-prepared Pd 3DPNN, further showing that the 3D porous network-like structure composited of joined-nanorods can be successfully fabricated using the combination strategy of interparticle fusion and the modulation of electrostatic repulsion during the nucleation and growth of metals.

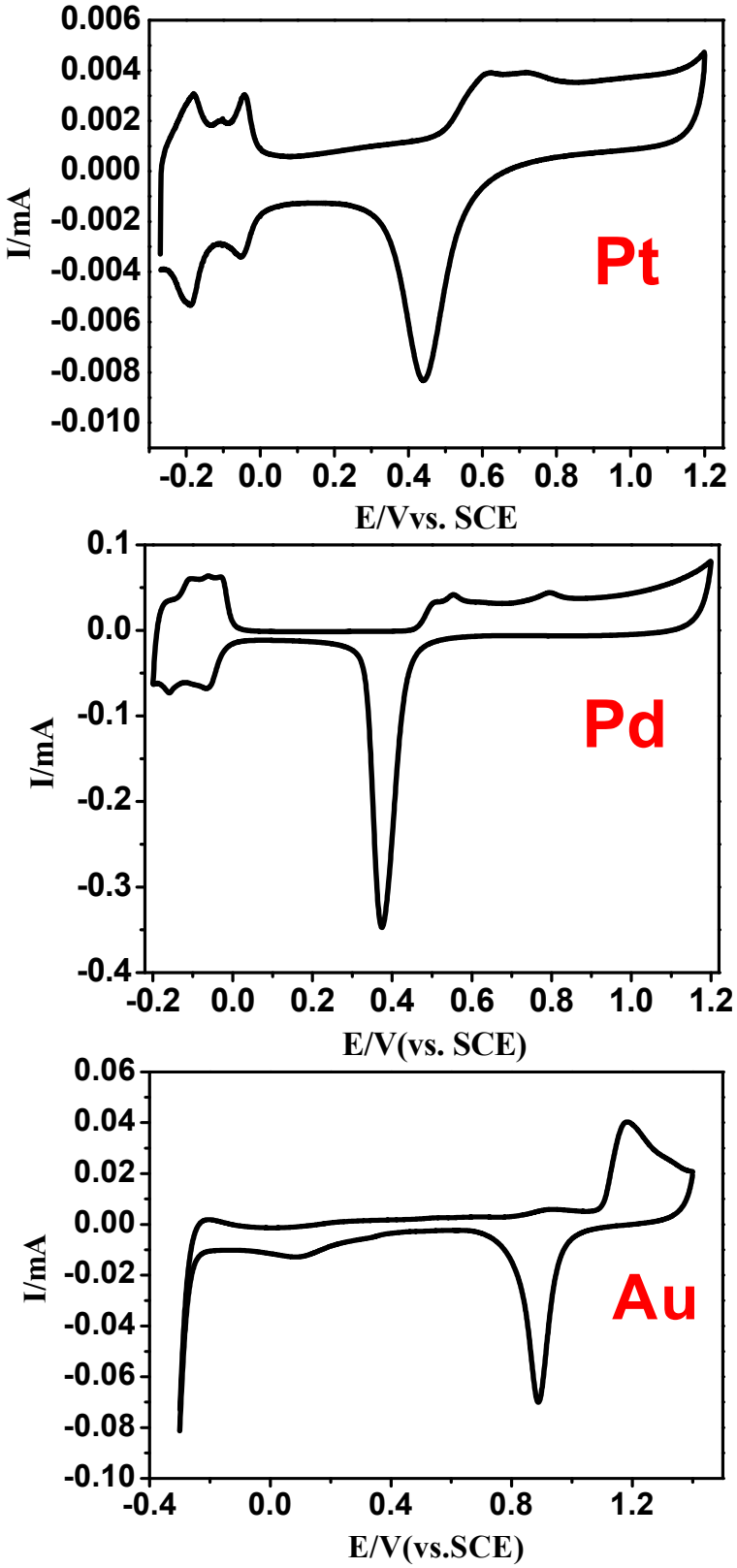

Figure S3. Cyclic voltammograms (CVs) of Pt, Pd and Au 3DPNN supported GC electrode, showing typical electrochemical behaviors of Pt, Pd and Au, similar to that of Pt particles (Zhang, B. et al. *Langmuir* **2005,** *21,* 7449-7455.), Pd particles (Sun, S. G. et al. *J. Am. Chem. Soc.* **2010**, *132*, 7580–7581.) and Au particles (Zhang, B. et al. *Langmuir* **2005,** *21,* 7449-7455.), respectively. The CV curves were recorded in 0.1M H_2SO_4 solution at a scan rate of 50 mV/s. The electrochemical measurements were

performed in a conventional three-compartment glass cell by using an electrochemical workstation (CHI 660, CH Instruments, Austin, TX). The network-structured metals or alloys were assembled on glassy carbon (GC) electrode by drop-coating to obtain the working electrode. A large platinum ring served as the counter electrode and a saturated calomel electrode (SCE) was used as the reference electrode. The working electrode was cleaned in 0.1 M H_2SO_4 by scanning the applied potential between -0.3 and +1.25 V at 100 $mV \cdot s^{-1}$ for 15 cycles before every measurement.

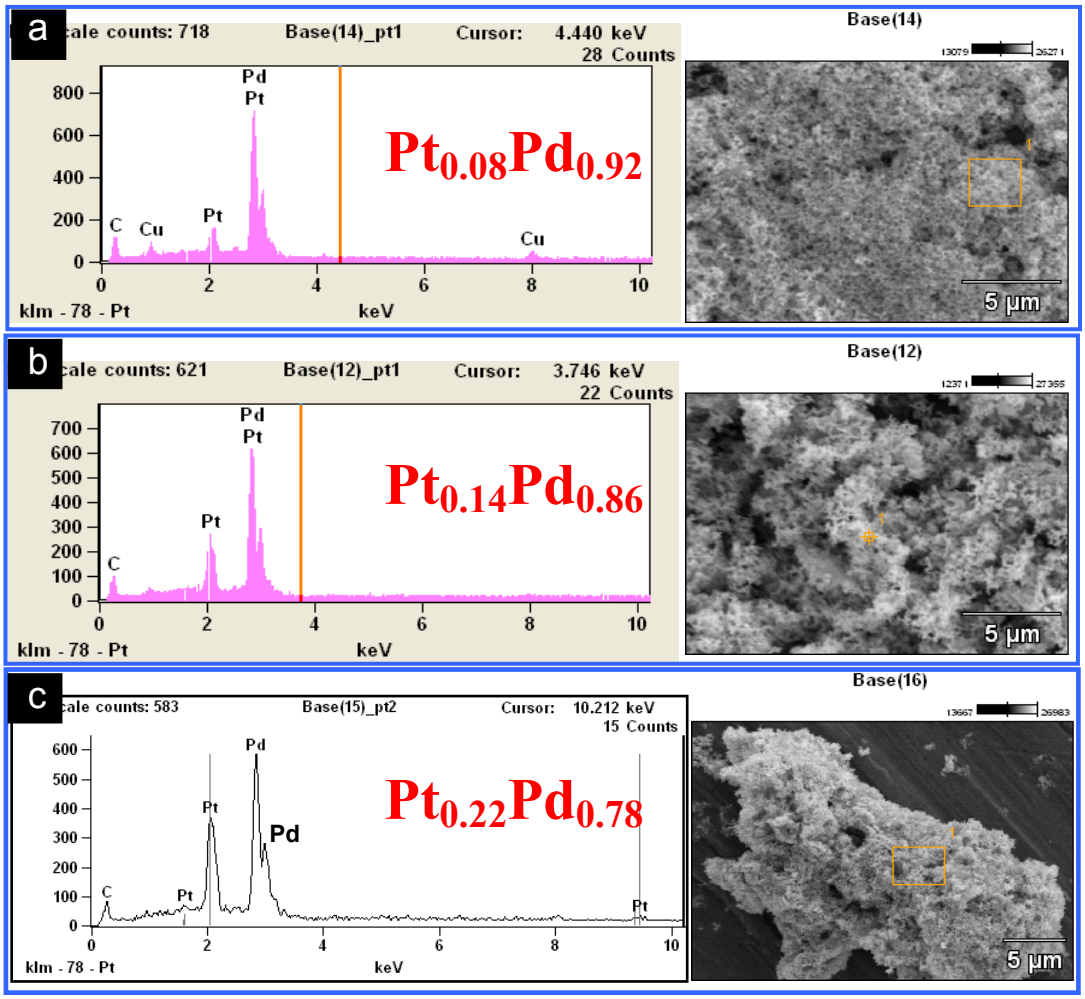

Figure S4. (a-c) EDX spectra and the associated SEM images of the as-prepared Pt-Pd alloy 3DPNN, showing that Pt-Pd alloy 3DPNN with modulating ratio of Pd to Pt can be fabricated through combining particle-fusion with the modulation of the electrostatic repulsion during the nucleation and growth of materials. In the EDX spectra, the detected Cu signals arise from the Cu foil on which the samples were deposited.

Table S1. Experimental parameters for the synthesis of Pd, Pt and Pt-Pd 3DPNN. [a] the composition of alloy is calculated according to the molar ratio of metal precursor added. [b] The composition of alloy is measured from the EDX spectra. It is clearly seen that the atomic ratios of Pd to Pt detected from EDX are in good accordance with the molar ratio of $Pd(OAc)_2$ to H_2PtCl_6 adopted (Entries 2-4).

Entry	H_2PtCl_6	$Pd(OAC)_2$	DTAB	HCHO	EG	H_2O	Composition[a]	Composition[b]
1	0	0.02 g	0.04g	2 mL	10 mL	10 mL	Pd	Pd
2	0.00165 mmol	0.01 g	0.04g	2 mL	10 mL	10 mL	$Pt_{0.10}$-$Pd_{0.90}$	$Pt_{0.08}$-$Pd_{0.92}$
3	0.00262 mmol	0.01 g	0.04g	2 mL	10 mL	10 mL	$Pt_{0.15}$-$Pd_{0.85}$	$Pt_{0.14}$-$Pd_{0.86}$
4	0.00495 mmol	0.01 g	0.04g	2 mL	10 mL	10 mL	$Pt_{0.25}$-$Pd_{0.75}$	$Pt_{0.22}$-$Pd_{0.78}$
5	0.005884 mmol	0	0.04g	2 mL	10 mL	10 mL	Pt	Pt

,

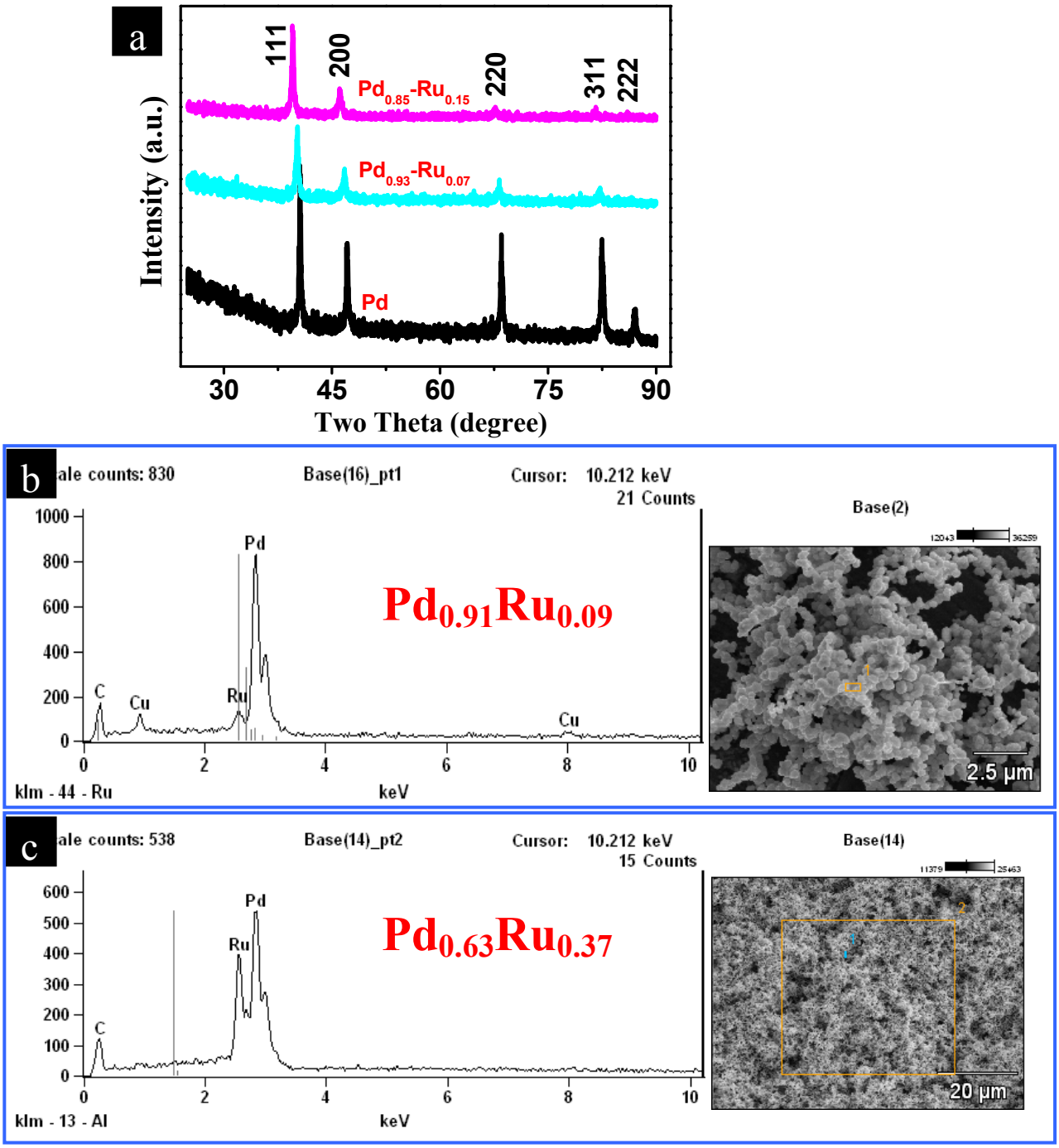

Figure S5. (a) XRD patterns of Pd, Pd-Ru alloy 3DPNN obtained in current work. It is clearly seen that the addition of $RuCl_3$ into the reacting solution of $Pd(OAc)_2$ leads to the obvious blue shift of (111) and (200) diffraction peaks in comparison with the XRD pattern of pure Pd. The atomic ratio of Pd to Ru was calculated according to the molar ratio of $Pd(OAc)_2$ and $RuCl_3$ added, suggesting the alloy structure of the as-obtained 3DPNN. These XRD patterns also show that the atomic ratio of Pd to Ru in Pd-Ru alloy 3DPNN can be adjusted by controlling the relative molar amount of metal precursors. (b-c) EDX spectra and the associated SEM images of the as-prepared Pd-Ru alloy 3DPNN. The atomic ratio of Pd to Ru detected from EDX (Figure S5b) is 0.91 to 0.09, in good accordance with the molar ratio of $Pd(OAc)_2$ to $RuCl_3$ (Pd:Ru=0.93:0.07) adopted. The EDX spectra in Figure S5b,S5c further confirm that the ratio of metals in alloy 3DPNN can be modulated. In the EDX spectrum, the detected Cu signals arise from the Cu foil on which the samples were deposited.

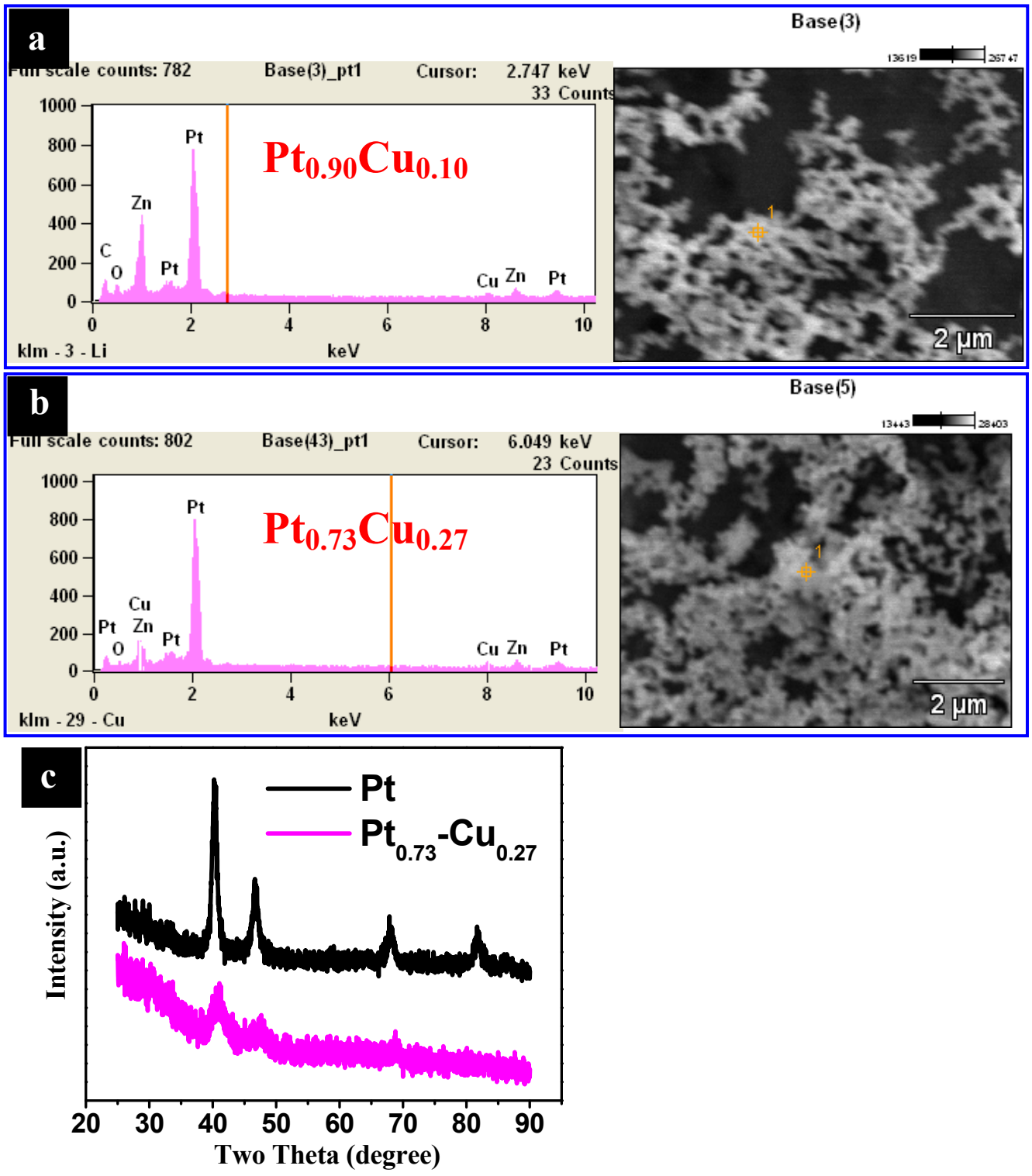

Figure S6. (a-b) EDX spectra and the associated SEM images of the as-prepared Pt-Cu alloy 3DPNN, showing that Pt -Cu alloy 3DPNN with modulating ratio of Pt to Cu can be fabricated here. In the EDX spectra, the detected Zn signals arise from the Zn foil on which the samples were deposited. (c) XRD patterns of Pt, $Pt_{0.73}$-$Cu_{0.27}$ alloy 3DPNN obtained in this approach. The slight blue shifts of (111) and (200) diffraction peaks of $Pt_{0.73}$-$Cu_{0.27}$ 3DPNN in comparison with the XRD pattern of pure Pt imply the alloy structure of Pt-Cu. This further confirms that the strategy to combine particle fusion with the modulation of electrostatic repulsion into the nucleation and growth of materials can be successfully extended to the synthesis of alloy 3DPNN.

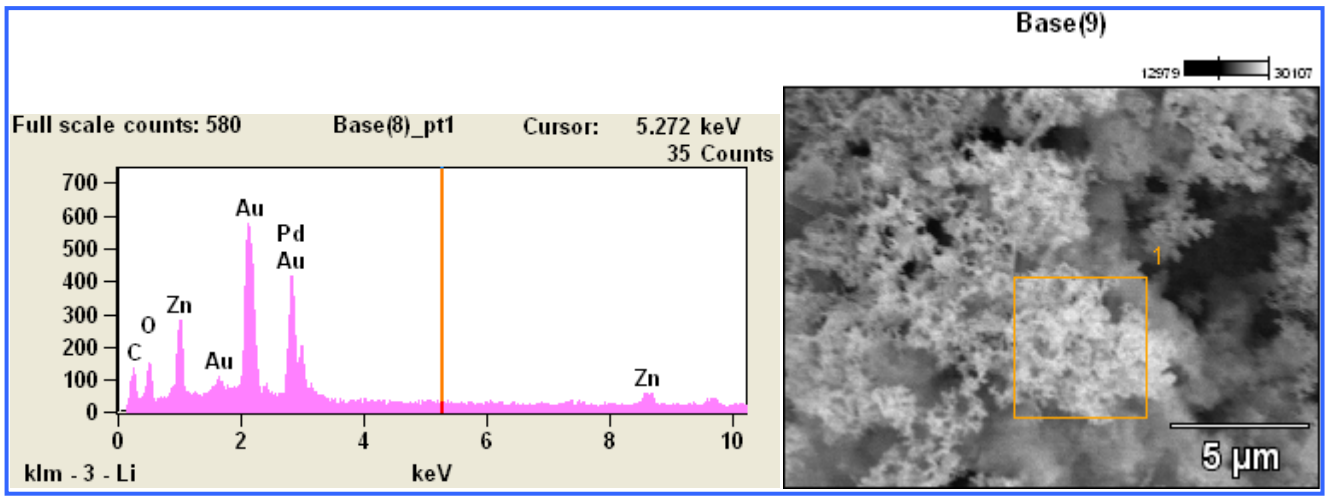

Figure S7 EDX spectrum and the associated SEM image of the as-prepared Au-Pd 3DPNN, showing the samples are composed of Au and Pd. In the EDX spectrum, the detected Zn signals arise from the Zn foil on which the samples were deposited.

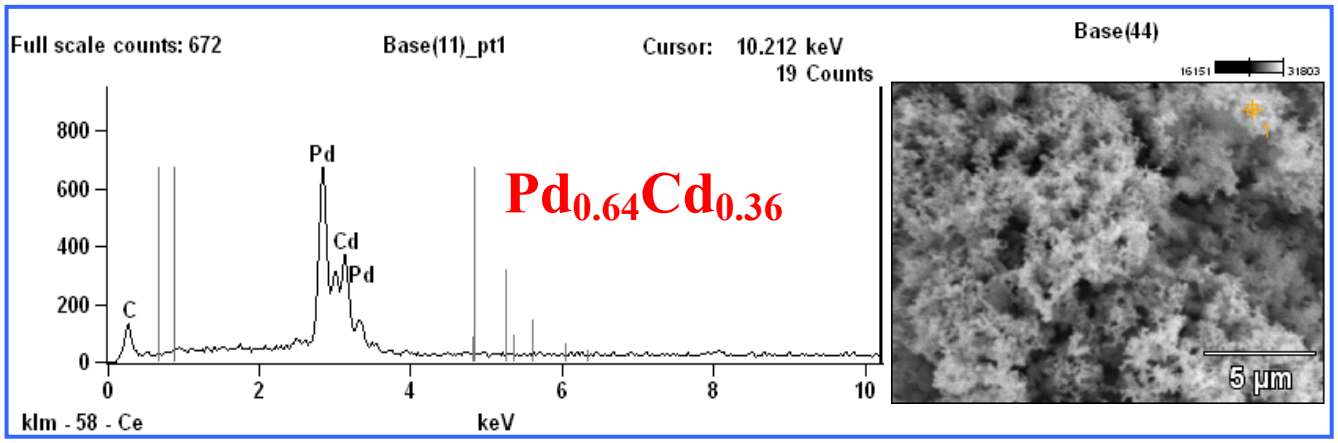

Figure S8. EDX spectrum of the as-prepared Pd-Cd 3DPNN, showing the samples are composed of Pd and Cd. However, only pure Pd network was generated when $Pd(OAC)_2$ and $CdCl_2$ were reduced by HCHO in this DTAB-assisted technique, which may be due to weak reducibility of HCHO for cadmium ions. When $HCOONH_4$ substitutes HCHO as the reducing agent, alloy can be successfully obtained, as shown in Figure S8, implying the fabrication of binary alloy porous network-like 3D nanostructures can be implemented using this DTAB-assisted one-step strategy in the presence of suitable reducing agent. Pd-Cd 3DPNN are expected to exhibit higher electrochemical hydrogen capacity due to the fact that the electrochemical hydrogen capacity of Pd nanoparticles can be improved through decorating Pd using Cd. (Adams, B. D.; Wu, G.; Nigro, S.; Chen, A. *J. Am. Chem. Soc.* **2009**, *131*, 6930-6931.)

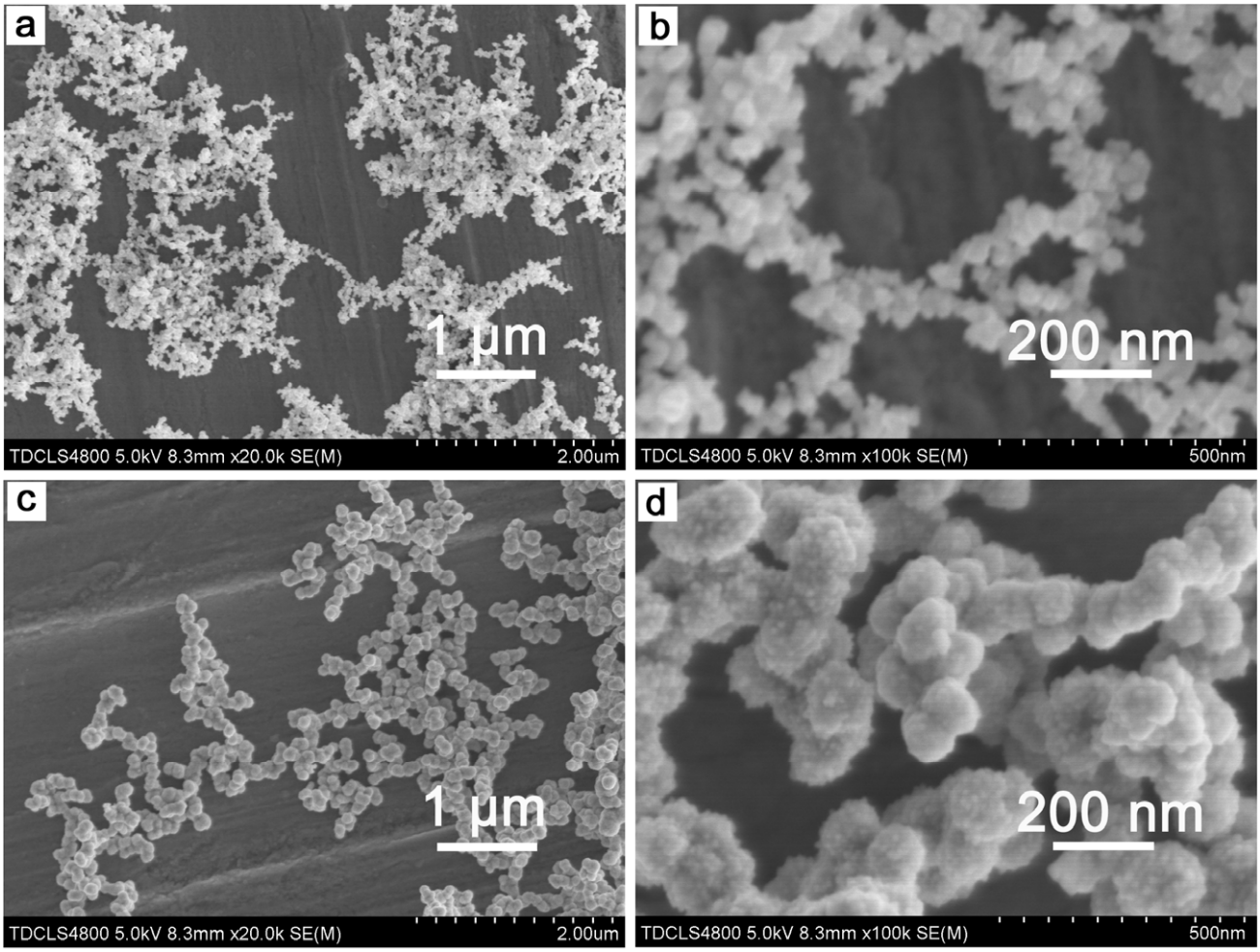

Figure S9. Low-magnification (a, c) and high-magnification (b, d) SEM images of two Pt 3DPNN prepared in the presence of different amounts of H_2PtCl_6: a-b) 0.12 mL 0.09194M H_2PtCl_6; c-d) 0.20 mL 0.09194 M H_2PtCl_6. When 0.08 mL of 0.09194M H_2PtCl_6 was adopted, the size of rod-like unit in Pt 3DPNN is 15-35 nm, as shown in Figure 2a,b, Figure 4 and Figure S2-1. The size of rod- and particle-like unit is 40-90 nm (Figure S9a-9b) when the amount of 0.09194M H_2PtCl_6 is increased to 0.12 mL. When the amount of H_2PtCl_6 added is increased to 0.2 mL, the size of unit in 3DPNN is 100-250 nm. These imply that the size of rod-like and particle-like unit in metal 3DPNN can be modulated by changing the molar amount of metal precursors adopted, which is important for exploring size-dependent physical or chemical properties.

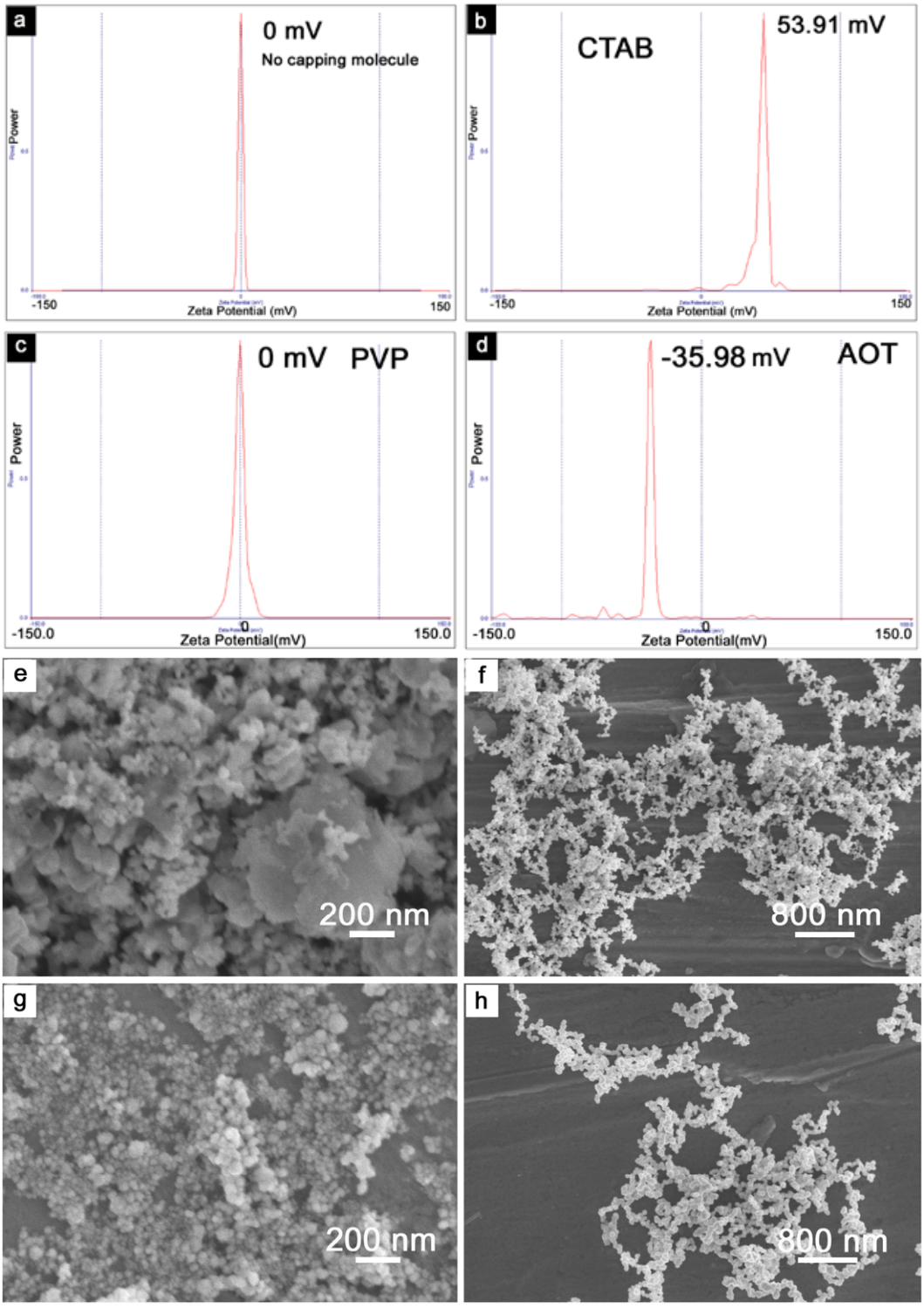

Figure S10-1. (a-d) Zeta potentials of different Pt samples prepared from 0.08 mL 0.09194 M H_2PtCl_6, 0.1 mL formaldehyde and 20 mL water in different capping agents: a) no capping agent; b) 0.02 g cetyltriethylammnonium bromide (CTAB); c) 0.02 g polyvinyl pyrrolidone (PVP, K30); d) 0.02 g bis (2-ethylhexyl) sulfosuccinate sodium salt (AOT). These results show that the samples are almost no charged in the absence of cation or anion surfactants or in the presence of no charged polymer—PVP. While the introduction of CTAB in reaction solution can make the samples be positively charged, AOT can make the samples be negatively charged. Thus, the addition of polar solvent or salt to modulate V_{elect} in the presence of AOT or CTAB to aqueous reacting solution should generate 3DPNN if our designed strategy (Figure 1 and Scheme S2) is reasonable. (e-h) SEM images of the Pt nanostructures prepared from 0.08 mL 0.09194 M H_2PtCl_6, 0.1 mL formaldehyde, 10 mL water and 10 mL ethylene glycol (EG)

in different capping agent. e) no capping agent; f) 0.02 g CTAB; g) 0.02 g PVP; h) 0.02 g AOT. In the absence of capping molecules, the samples are aggregates because V_{elect} is very weak (no charged), as shown in Figure S10-1e. While in the presence of CTAB or AOT, the addition of EG or salt can result in the decrease of V_{elect} according to Derjaguin-Landau-Verwey-Overbeek (DLVO) theory (Israelachvili, A J. Intermolecular & Surface Forces, Academic Press, London, **1997**.) and calculated equation of V_{elec} that Wang and his coworker suggested (Zhang, H.; Wang, D. *Angew. Chem. Int. Ed.* **2008**, *47*, 3984–3987), and produce 3DPNN (Figure S10-1f, 10-1h). When cation or anion surfactant is replaced by PVP, the obtained samples are dispersed NPs. This suggests that the introduction of charged molecules to cap as-prepared nuclei or seeds as well as the modulation of V_{elec} is significant to the production of metal 3DPNN.

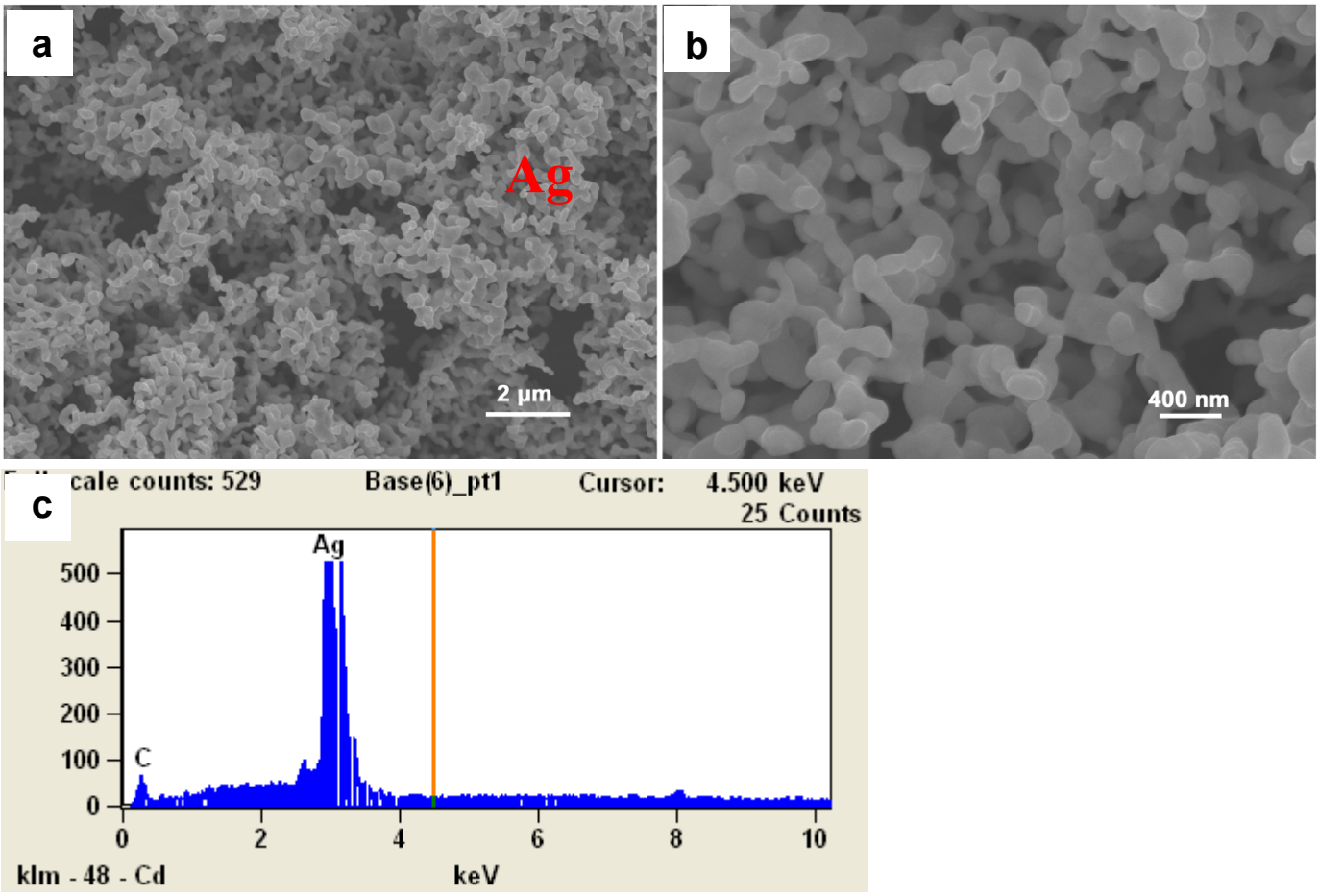

Figure S10-2. SEM images (a, b) and EDX spectrum of Ag 3DPNN prepared when AgOAC is reduced by using HCHO in the presence of aminoacetic acid (NH_2CH_2COOH), a negatively charged molecules in base solution (It is known that amido or mercapto groups are easily adsorbed on the surface of noble metal, carboxylic acid can transformed into negatively charged $–COO^-$. But molecules containing mercapto group can react with metal ions to generate metal sulfides. Thus, organic molecules with amido and carboxylic groups can adsorb onto metal nuclei and seeds during the reduction of the metal precursors, and make the nuclei and seeds negatively charged at suitable pH valuation solution. Aminoacetic acid, the simplest one among such charged capping molecules, is adopted to replace anion or cation surfactants used in Figure 1 and Figure S10-1.) . These results suggest that metal 3DPNN can also be fabricated by correlating the electrostatic repulsion with the heat-induced fusion using other charged molecules, confirming the charging function of DTAB or other anion surfactants.

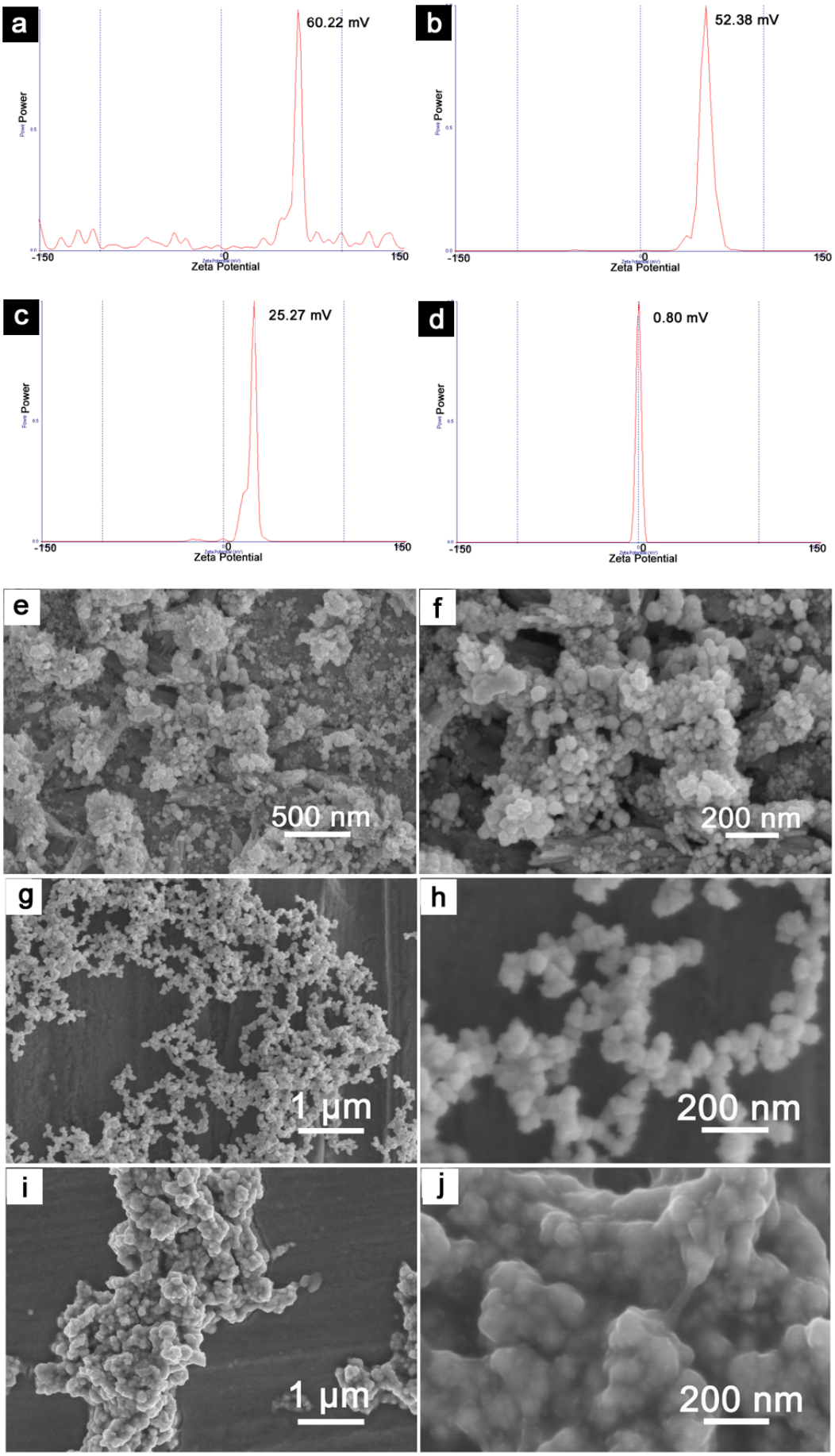

Figure S11-1. (a-d) Zeta-potentials of DTAB-modified Pt nanostructures prepared after adding different

amount of NaCl to refluxing solution. (a) 60.22 mV: no NaCl, (b) 52.38 mV: 100 μL 1M NaCl, (c) 25.27 mV: 600 μL 1M NaCl, (d) 0.80 mV: 1200 μL 1M NaCl. This shows that positively charged amount of DTAB-modified NPs can be decreased with increasing the addition amount of salt, that is, the addition of salt will lead to the decrease of electrostatic repulsion potential (V_{elect}) of charged nuclei and seeds. (e-j) low-magnification (e, g, i) and high-magnification (f, h, j) SEM images of Pt nanostructures prepared from 0.08 mL of 0.09194 M H_2PtCl_6, 0.02 g of dodecyltrimethylammonia bromide (DTAB), 0.1 mL of formaldehyde and 20 mL of water in the presence of different amount of NaCl. (e-f) no NaCl, (g-h) 600 μL 1M NaCl, (i-j) 1200 μL 1M NaCl. When the reacting solution was treated at 150 ºC, H_2PtCl_6 can be reduced to Pt(0). DTAB molecules will adsorb on the surface and make the as-formed Pt nuclei and seeds be positively charged. In the absence of NaCl (or polar solvent with lower dielectric constant), the strong V_{elect} inhibits the aggregation and fusion of the Pt nuclei, which used as the seeds for the following Ostwald growth ripening(Scheme S2a), and thus leads to the formation of dispersed Pt NPs (Figure S11-1e and Figure S11-1f). It is clearly shown that the dispersed Pt NPs are obtained in the absence of NaCl due to the fact that V_{elect} is much stronger than the van der Walls attraction (V_{vdw}). The addition of salt can lower V_{elect}, as displayed in Figures S11-1a--S11-1d. When more salt was added, the chain-like nuclei may appear (Scheme S2b), and further fuse into 3DPNN, as described in Scheme S2b and shown in the SEM images in Figure 2a,b, Figure S11-1g, and Figure S11-1h. When the salt added is over 1000 μmol, the stronger V_{vdw} (>3 V_{elect}) drives the as-formed DTAB-modified nuclei to aggregate and merge into bigger particles (Scheme S2c, Figure S11-1i and Figure S11-1j). These results show that 3DPNN can be successfully fabricated by modulating V_{elect} of charged nuclei and seeds through adding salt to the initial reaction solution. Note that the addition of polar solvent with lower dielectric constant to control V_{elect} is similar to that of salt effect. The reason why the role of NaCl to modulate V_{elect} is chosen as the case is mainly due to the fact that the change of Zeta potential with the addition of NaCl is easier to be monitored.

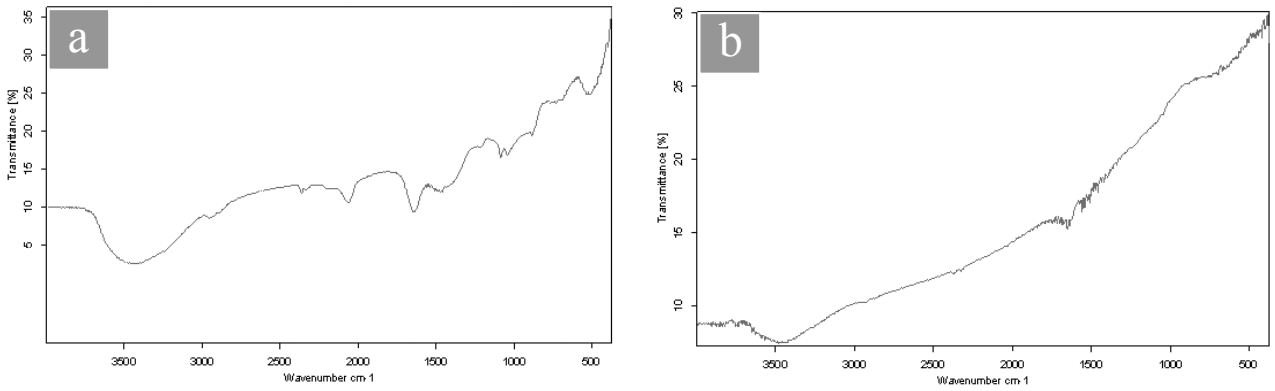

Figure S11-2. FTIR spectra of the as-prepared Pt 3DPNN after rinsing for different times with ethanol, acetone, and water, respectively. (a) two times, (b) eight times. These signals from Figure S11-2a can be attributed of DTAB, indicating DTAB molecules were adsorbed on the surface of Pt. However, no obvious signals can be detected after washing for eight times (Figure S11-2b), indicating that the capping molecules on Pt 3DPNN can be removed through repeated rinsing.

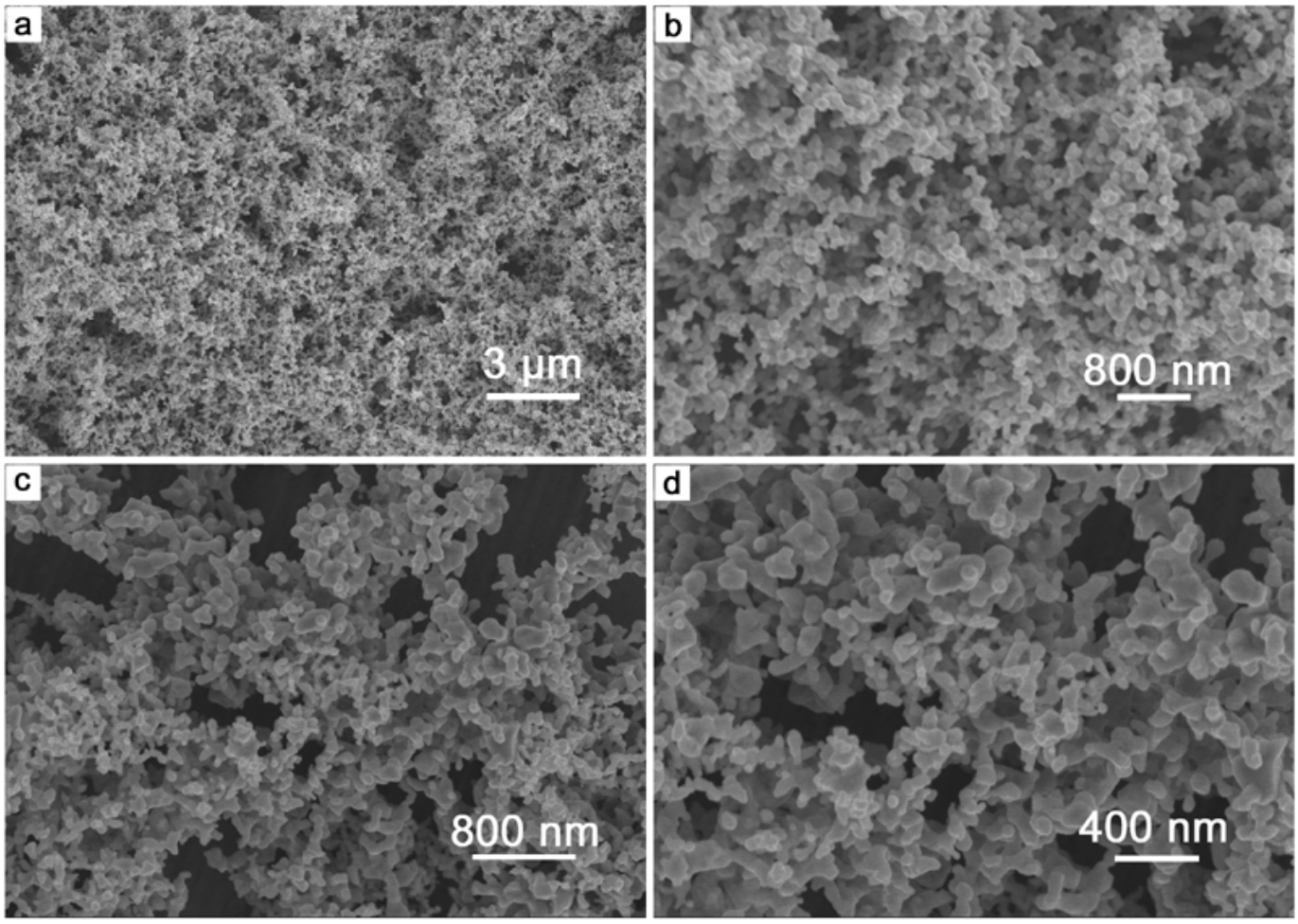

Figure S11-3. SEM images of Pt 3DPNN prepared from 0.08 mL 0.09194 M H_2PtCl_6, 0.1 mL formaldehyde, 0.02g DTAB, 10 mL H_2O and 10 mL EG at different temperatures. (a-b) 150 ºC; (c-d) 200 ºC. When the reaction temperature is lower than 80 ºC, no obvious precipitates are collected. 3DPNN will appear when the temperature is over 100 ºC. At 150 ºC, the rod-like units in 3DPNN are relatively uniform, as shown in Figure 2a,b, Figure S11-3a and Figure S11-3b. The reaction under the same condition but at lower temperature generates the mixture of 1D chains and NPs. The high temperature facilitates the fusion between NPs or chains and promotes the formation of 3DPNN. But at above 200 ºC, serious and quick fusion is not conducive to the yield of 3DPNN. As displayed in Figure S11-3c and Figure S11-3d, the rod-like units in Pt network are not uniform.